Behaviour of macroscopic rigid spheres in Poiseuille flow

Part 1. Determination of local concentration by statistical analysis of particle passages through crossed light beams

By G. SEGRÉ† AND A. SILBERBERG

Weizmann Institute of Science, Rehovoth, Israel

(Received 6 November 1961 and in revised form 16 March 1962)

An apparatus is described for determining particle passages through any selected point on a tube cross-section. The method depends on the simultaneous blocking out of two mutually perpendicular light beams by a particle passing through their common region. The coincidence is registered and counted electronically. At higher particle concentrations coincidences are also registered arising from a pairwise occupation of the light beams by two particles. An analysis is presented showing that these pair coincidences can be allowed for exactly in terms of experimentally measurable quantities.

The reliability and reproducibility of the method is discussed and illustrated by examples from sphere suspensions in Poiseuille flow.

1. Introduction

Radial displacements of spherical rigid particles carried along in Poiseuille flow have been suspected in the past. Several experimental observations tending to show their existence have been reported and theoretical reasons advanced to account for the phenomena. All theoretical discussions so far have predicted an inward shift of particles and for this, as well as for reasons of convenience, most observations involved a study of the concentration changes in layers nearest the tube wall.

It was our aim to make the observation of particle motion as direct as possible and we used for this purpose an optical scanning device consisting of two mutually perpendicular light beams whose intersection could be made to test out all points on the tube cross-section. Photoelectric transducers and electronic counting circuits were used to register particle passages. A statistical analysis of the counts obtained in this way enabled us to derive the necessary data for an analysis of single particle behaviour. We had to distinguish between the blocking of both channels by a single particle ('hits'), and the blocking of the two channels by the presence simultaneously of two particles, one in each channel ('pair coincidences'). It was the former which we wanted to know but our direct measurements gave us their sum. A theory was developed (see § 6) for this type of coincidence counting from which it appeared that simple additional measurements can be made to separate the 'hits' from the rest of the counts.

† On leave from Cartiera Vita Mayer and Co., Milan, Italy.

In the following we shall give, first of all, a detailed description of the experimental arrangement; the flow system in § 2, and the optical scanning device and photoelectric transducer in § 3. The nature of the pulses which the apparatus yields is discussed in § 4 and the method of counting and analysing them follows in § 5.

In § 7 we describe a way of deriving more precisely defined concentration distributions from results which, due to our type of coarse scanning, are averages over relatively large regions. The controls we have carried out and the degree of coherence and reproducibility which can be obtained by this method are discussed in § 8.

In Part 2 (Segré & Silberberg 1962), the theoretical background will be analysed, and the results presented in full and discussed. It will be shown that the particles are displaced radially outwards from the centre and inwards from the wall, and that a stationary build up of concentration occurs at a radial position at about two-thirds tube radius ('tubular pinch effect') (Segré & Silberberg 1961).

2. The flow system

A schematic picture of the flow apparatus is given in figure 1.

The flow tube is composed of two pieces of glass tubing, carefully chosen for their uniformity, having an internal diameter of $11{\cdot}2 \pm 0{\cdot}2$ mm.† The two pieces are situated one above and one below the optical system. The length of these pieces may be changed by substituting different tubes in order to perform the measurements at different distances l from the inlet. For a given total length of the tube $l_1 + l_2$ (see figure 1) measurements were made alternately in downward flow and in upward flow, giving results at different values of l, $l = l_1$ and $l = l_2$ respectively.

Two containers are connected to the flow tube, an upper container R_1 and a lower one R_2, the transition section between tube and container being given a conical shape. The purpose of the containers is twofold, to feed the tube and to assure uniformity of the suspension.

The suspensions were made up of polymethylmethacrylate spheres in media of equal density and different viscosities (17 to 400 cP), prepared by mixing glycerine, 1,3-butanediol and water in various proportions. The particles were closely matched in diameter by passing them through a sieve, composed of a slit whose gap could be accurately adjusted. Calibrated photographs were used to determine the size distribution and the mean diameter of each fraction.

Although the stability of the suspension is assured by careful matching of the density of the liquid with the density of the particles (kept always within 1‰ of each other) concentration inhomogeneities are produced in the containers after passage of the sample volume through the tube. It is necessary therefore to employ stirring, and the liquid in the containers was generally kept in constant motion.

The conical mouth sections at the ends of the tube and the system of applying the pressure to the suspension, either through the free meniscus in the upper

† In our preliminary note (Segré & Silberberg 1961) the inner tube diameter was erroneously given as 11·6 mm.

container or through a thin flexible membrane in the lower one, is intended to feed the tube with a suspension as homogeneous as possible, in a flow pattern as close to the ideal as could be attained. A column of water is used to counterbalance the suspension across the membrane in container R_2.

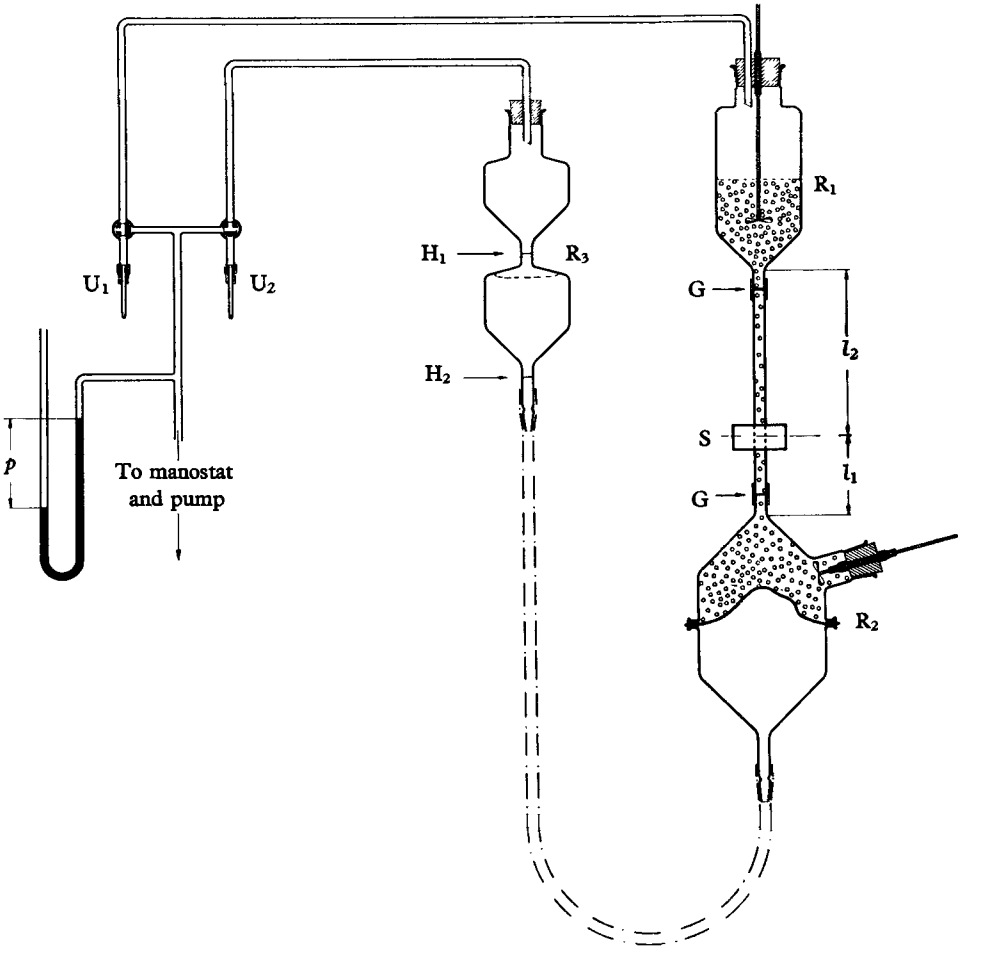

FIGURE 1. Schematic view of the flow system. R_1, R_2, R_3, containers; S, scanning device; G, joints; U_1 and U_2, nozzles for control of pressure p; H_1 and H_2, pipette marks.

The flexible tube containing this water counterweight terminates in the container R_3, which measures the flow volume v, between the two marks H_1 and H_2. The volume actually pushed into the tube in an experiment was about 20 % larger than the measured volume due to the fact that the motion was started above the mark H_1 and was stopped below H_2. This prevents the initial and final phases of the motion, where large accelerations are present, from being included in the measurement. The actual time of flow T corresponded to the interval elapsing between the passage of the meniscus from H_1 to H_2. The volume of flow was 660 cm^3 and the time of flow varied between 7·5 and 120 sec depending on the pressure difference applied, the liquid viscosity and the length of the flow tube.

The height of the container R_3 is regulated in such a way that the liquids are in barostatic equilibrium at a position halfway between H_1 and H_2. The average hydrostatic head is thus zero. The constant-pressure system designed to provide the driving head is composed of a water suction pump, a mercury manostat, a mercury barometer and a large aspirator acting as pressure stabilizer. This system may be connected to one of the containers R_1 or R_3, while the other is connected to the atmosphere through suitable nozzles U_1 or U_2. The choice of the nozzle and of the pressure p determines the flow velocity which will be obtained.

At the inlet of the tube, after a short transition length, the liquid reaches the parabolic, axially symmetric velocity profile, corresponding to Poiseuille motion; we shall show in § 8 the experimental evidence for this fact.

3. The optical system

Two strong perpendicular light rays, well collimated, for the scanning of the chosen cross-section of the tube, were obtained by means of the system shown schematically in figure 2. The lamp A is a Sylvania concentrated-arc lamp of

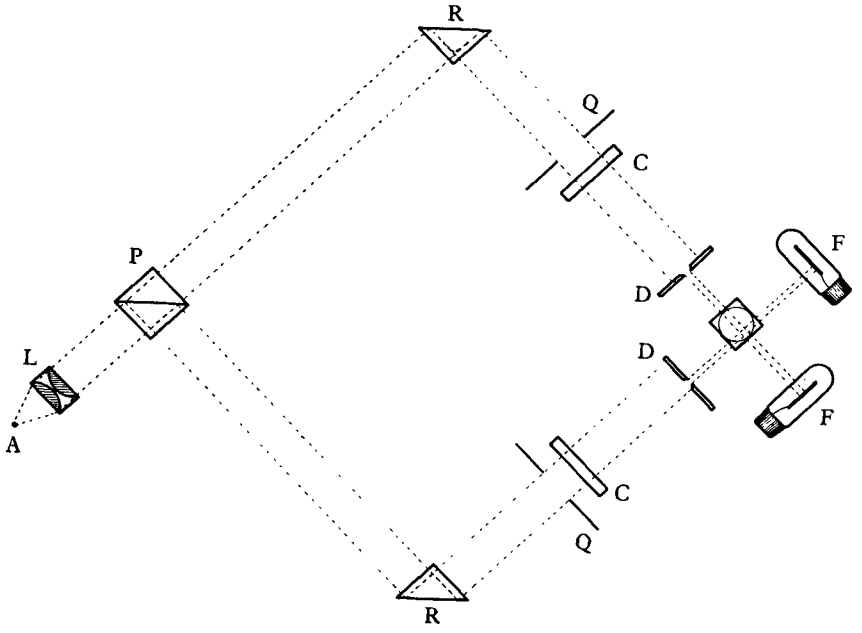

FIGURE 2. Schematic view of optical system. A, Light source; L, collimating lens; P, semi-transparent prism; R, reflecting prisms; Q, apertures; C, cylinder lenses; D, movable square diaphragms; F, photocells.

25 W, fed from a battery of accumulators; the point crater coincides with the focus of the lens system L (Xenon F: 1·5; f = 2·5 cm) which gives a circular parallel beam of about 2 cm diameter. The light is split into two perpendicular beams by means of the semi-transparent prism P. A totally reflecting prism bends each of these two beams towards the scanning device. A square aperture Q outlines a pencil of light which afterwards is concentrated (squeezed) in the vertical direction by means of a cylinder lens C.

We obtain in this way a very strong luminous image, less than 2 mm high and more than 1 cm wide, on the two faces of the scanning prism. Figure 3 shows this prism decomposed into its elements. At the centre we have the scanning section S, which consists of a Perspex segment 1·5 mm thick provided with a square hole of length of side equal to the inner tube diameter, within whose thickness the light rays are conveyed without distortion. It is believed that the small local deviation from a cylindrical cross-section in the tube does not affect the flow pattern. On the other hand, the use of such a plane parallel-walled section made it possible to

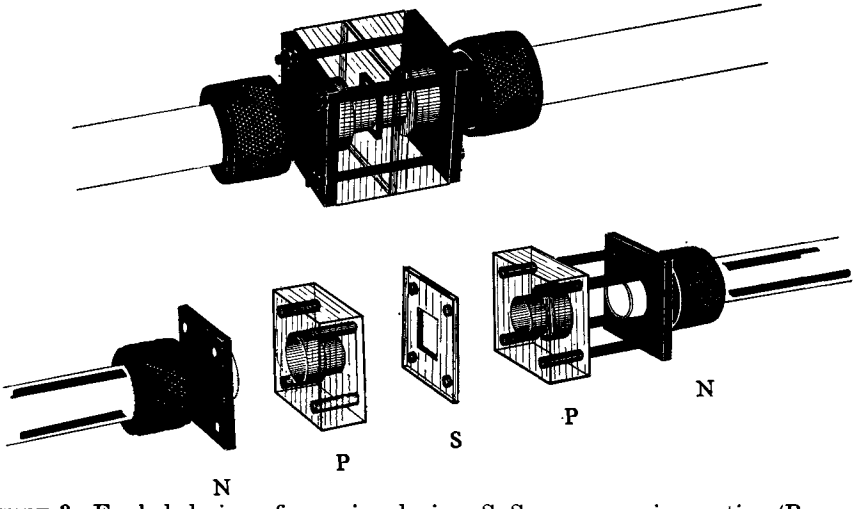

FIGURE 3. Exploded view of scanning device. S, Square scanning section (Perspex); P, Perspex blocks; N, glass tube seals (brass).

obtain uniform precise scanning of all positions on the cross-section. On the incident sides of S are two diaphragms D (figure 2) provided with a square hole of side 1 mm which may be displaced horizontally with the help of a micrometer screw. We shall use a rectangular (x, y, z)-co-ordinate system, based on the centre of the scanning section, such that the z-axis points in the direction of the mean flow and the x- and y-axes lie in the plane of the scanning section parallel to its sides.

A scale divided in half millimetres and a magnifying glass help in determining the position (x, y) of the diaphragm centre, with a precision of $\pm 0{\cdot}2$ mm. On the emergent faces of the prism, black masking tape eliminates stray light. The resulting ray is therefore sufficiently collimated to ensure that the sensitive volume, for any of the two scanning directions, has the shape of a prism having as axis a diameter or a chord of the cross-section of the flow tube.

The optical system is completed by the two phototubes F (figure 2) (type 5652) and a series of gray filters (not shown) with which to control the light intensity of the two beams. These may be regulated jointly or separately, to compensate intensity variations in the lamp or a lack of symmetry in the two optical paths.

The particles to be counted, being of transparent polymethylmethacrylate, needed to be treated in order to increase the contrast with the suspending liquid. We achieved good visibility by roughening the surface of the particles with a mixture of HCl, HNO_3 and water in suitable proportions. Only for the smallest

particles were the results not completely satisfactory. In order not to damage their shape, very rapid treatment was given and a portion of the particles remained too clear to be counted.

4. Character of the pulses

When no portion of a particle lies in one of the beams going through the flow tube the corresponding photocathode receives the total luminous flux, and at the terminals of the load resistor in the cell circuit we have the potential difference H_0 (figure 4).

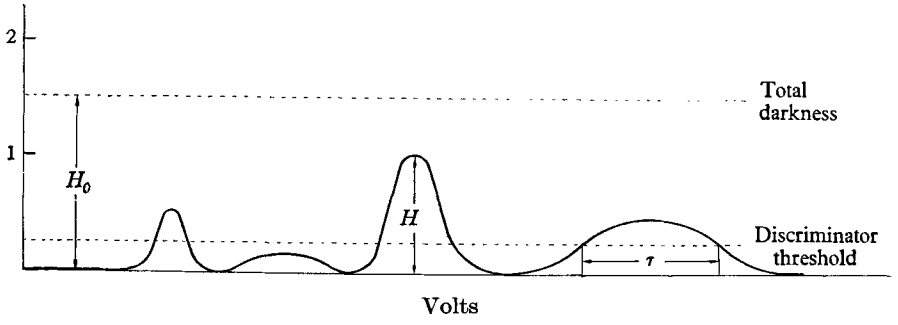

FIGURE 4. Pulse characteristics. H_0, Maximum photoelectric potential; $H_0 - H$, photoelectric potential during pulse; τ, pulse duration.

When a spherical opaque particle, having a diameter of about 1 mm, crosses the light beam, a part of the light will be intercepted. The shadow will initially increase until it reaches a maximum, and then will decrease again to zero upon the completed egress of the particle from the light beam. In order to obtain a signal it is sufficient that the centre of the particle follows a trajectory passing at a distance $\delta < a + \frac{1}{2}d$ from the beam axis (see figure 5), where a is the radius of the particles and d the width of the light beam, that is the aperture of the diaphragm (1 mm). The need for eliminating the background noise, and the desire sometimes to reduce as much as possible the width of the sensitive area, induces one to use a more or less high level of discrimination, that is to bias the electronic circuit in such a way that signals which do not reach a prescribed height are eliminated. The 'sensitive region' outlined in this way is the region which a particle must cross in order that its passage will be registered. Its width $\Delta x \leqslant d + 2a$ thus depends not only on the dimensions of the particles and of the diaphragm but also on the light intensity and on the discrimination threshold employed. The smallest Δx, and therefore the best resolution, could be obtained in principle by matching the diaphragm aperture to the particle diameter, and by using a high level of discrimination. However, small fluctuations in this level would produce large relative errors in the counts. In general we preferred to use rather wide Δx, for which reproducibility was much more satisfactory.

The second feature of the signal which interests us is its duration τ, defined as the time that it remains above the discrimination level (see figure 4). This magnitude depends in the first place on the parameter δ as well as on the other variables determining the height of the signal, and in the second place on the

velocity of the particles, which we assume coincides, in first approximation, with the local fluid velocity, $V(r) = 2V_m[1-(r/R)^2]$. Here V_m is the average velocity of flow, r is the radial particle position and R is the tube radius.

We now consider the 'sensitive volume', that is the volume where the presence of a particle in the beam produces a shadow above the threshold level. The 'sensitive volume' is a prism with a rather complex cross-section, having in the z direction a variable thickness Δz, roughly equal to Δx at the centre but much smaller at the sides.

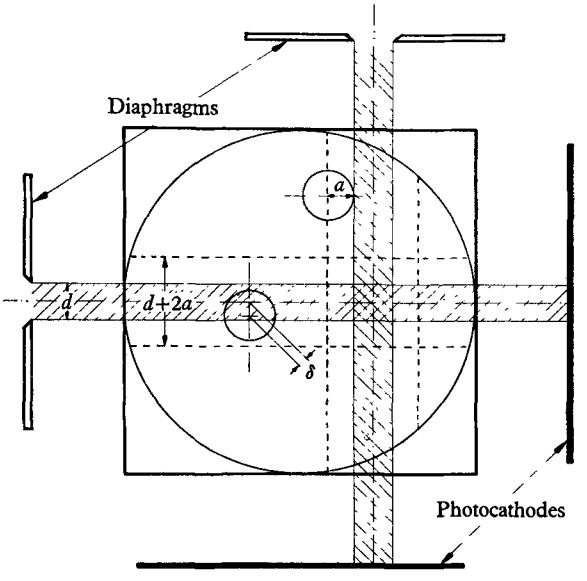

FIGURE 5. Details of light paths in scanning section. d, Diaphragm opening; a, particle radius; δ, particle position relative to beam axis.

From a statistical point of view we are interested in the number of particle passages through each of the sensitive regions in the (x, y)-plane, numbers which we will call $N_s(x)$ and $N_s(y)$ depending upon the two observation directions. In addition we want to know the number N_c of coincidences, that is of overlapping pulses in the two channels.

In the second place we are interested in knowing the 'presence number' of particles in the sensitive volume, which is measured by the fraction of the time that this volume is occupied by at least one particle. This presence number, or occupation probability, $p(x)$ or $p(y)$ for each channel respectively, may be obtained by summing the durations τ of all the signals in that channel for a given time of flow T:

$$p = (\Sigma\tau)/T.$$

These are the magnitudes that the electronic circuit should measure.

5. The electronic circuit

The electronic circuit is essentially a coincidence circuit, which has the function of detecting and counting the simultaneous presence of a signal at the output of both phototubes. The tube performing this function is a pentode 6 BN 6 whose two

control grids receive the signals corresponding to the two light beams. The discrimination level for the signals is set by the amount of negative bias given to these grids and is controlled by suitable potentiometers.

The detection of the 'singles', that is of the pulses generated by any one of the two phototubes, is performed by a pentode of the same type, one of whose control grids is grounded, corresponding to a permanent signal on that grid. To simplify the construction, only one detector of singles has been employed, and is used alternately with one or other of the two photocells.

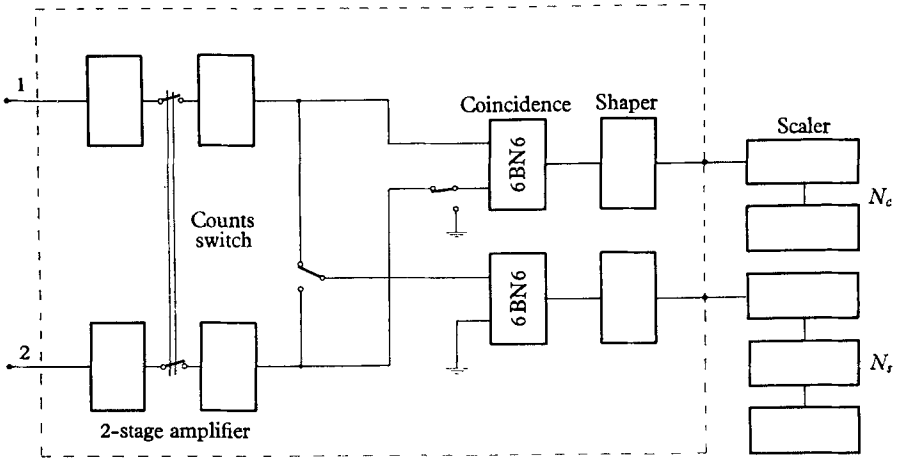

FIGURE 6. Block diagram of counting circuit.

In order to measure the total duration of the signals, we again make use of the coincidence circuit, by sending one of the signals to input 1 and a square wave of known and sufficiently high frequency to input 2; the signal to be measured acts as a gate on the periodic oscillation, allowing the passage of a number of waves proportional to the pulse duration. Also this measurement is performed alternately for each one of the two observation directions.

The diagram of figure 6 shows the different components of the circuit. From inputs 1 and 2 the signals are amplified by a double triode, the counts switch being placed between the two amplification stages. The pulses, amplified from about 1 V to about 40 V, go to the coincidence tube, while one, at will, of the two channels is connected to the 'singles' circuit. This is quite similar to the coincidence circuit but for the already-mentioned grounding of one of the control grids. By means of a switch, one of the grids of the coincidence tube may also be grounded and we obtain two identical circuits for calibration purposes.

The signals emerging from the 6BN 6 are squared, differentiated, rectified and then fed to a double scaler, one section of which counts the coincidences N_c and the other the singles N_s. The same scaler, with the two sections in cascade, to get a higher counting capacity, measures the 'presence number', by counting the number of waves admitted by the 'gate' action already described.

These circuits worked very satisfactorily; great care was taken to avoid pick-up of external noise, double counting due to overshooting of the signals and noise due to the counts switch operation.

6. Statistical analysis of the counts

If the concentration of the particles in the flow tube were constant everywhere, the number of particles passing a given point in unit time would be proportional to the velocity of the suspension there. As velocity has a parabolic distribution across the tube, if the suspension is Newtonian and the flow laminar, the number of particle passages should also be distributed according to a parabolic law. Our experiments show that a parabolic law of particle passages holds in general near the mouth of the tube for a short section beyond the inlet length. Farther away

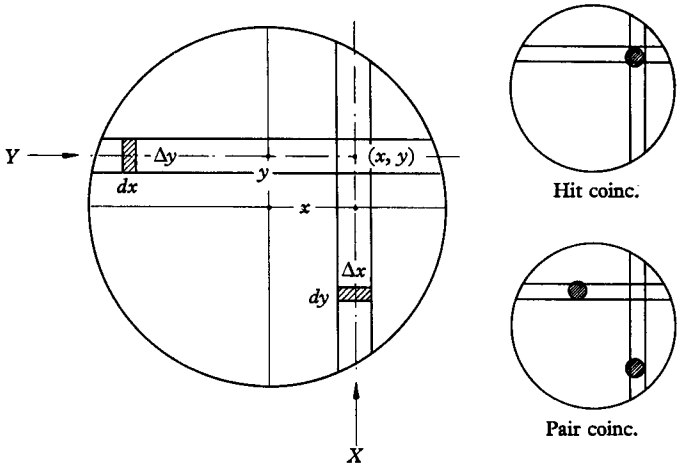

FIGURE 7. Channel characteristics.

from the mouth very different distributions are observed. As the Poiseuille character of the flow can be assumed to hold, in view of the fact that one is working with highly diluted suspensions and at rather low Reynolds numbers, our results tend to show that concentration rearrangements are taking place when the spheres move deeper into the tube. The purpose of this and the next section is to show how these concentration changes can be measured with the arrangement described.

Let us consider a point (x, y) on the cross-section of the tube. This point is determined by a light ray parallel to the y-axis, at a distance x from the centre, and by a similar ray orthogonal to it, at a distance y from the centre. The rays mark the axes of the sensitive regions of width Δx and Δy respectively which in the following we shall designate as 'channel X' or 'channel Y' (see figure 7). 'Occupation' of the channel by a particle implies that its centre is situated within it and that this presence will be detected electronically (see definition of Δx in § 4).

The electronic network counts a 'coincidence' every time that (at least) one particle occupies channel X while (at least) one (the same or another) particle occupies channel Y. The coincidence is registered when such a situation first arises, independently of the subsequent duration of the simultaneous occupation. Let us call 'hit coincidences' those due to a single particle, 'pair coincidences' those due to two particles.

If the concentration were sufficiently low, we would regard pair coincidences as extremely unlikely and the total count of coincidences could be regarded as 'hits'. For practical reasons, still to be discussed, such low concentrations could not be worked with. A statistical analysis will now be given showing that pair coincidences can be evaluated indirectly from the experiment, provided that we may assume that the simultaneous occupation of the channels by three particles is so unlikely as to be negligible. The range of concentrations which we have used satisfies this condition, and we shall therefore neglect third-order terms.

Let us now define two functions at each point of the cross-section of the tube, a function

$$n(x,y) = V(x,y)\,C(x,y), \tag{1}$$

representing the number of particles per unit cross-section per second which pass (x,y), where $V(x,y)$ is the local velocity of the fluid and $C(x,y)$ the local concentration of particles, and a function

$$\begin{aligned}\omega(x,y) &= \tau(x,y)\,V(x,y)\,C(x,y)\\ &= \tau(x,y)\,n(x,y),\end{aligned} \tag{2}$$

representing the probability density that a particle will occupy the sensitive region of height Δz, where $\tau(x,y)$ is the time spent by a particle in traversing the sensitive region at (x,y), so that

$$\Delta z = \tau(x,y)\,V(x,y). \tag{3}$$

The probability ω_c of the simultaneous occupation of the sensitive region at two points **1** and **2** is thus given by

$$\omega_c(\mathbf{1},\mathbf{2}) = \omega(\mathbf{1})\,\omega(\mathbf{2}) = \tau(\mathbf{1})\,n(\mathbf{1})\,\tau(\mathbf{2})\,n(\mathbf{2}). \tag{4}$$

If $n_c(\mathbf{1},\mathbf{2})$ is the number of coincidences which arise per second between points **1** and **2**, and $\langle\tau(\mathbf{1},\mathbf{2})\rangle$ is the average duration of a coincidence we have also

$$\omega_c(\mathbf{1},\mathbf{2}) = n_c(\mathbf{1},\mathbf{2})\,\langle\tau(\mathbf{1},\mathbf{2})\rangle. \tag{5}$$

But

$$\frac{1}{\langle\tau(\mathbf{1},\mathbf{2})\rangle} = \frac{1}{\tau(\mathbf{1})} + \frac{1}{\tau(\mathbf{2})}, \tag{6}$$

so that it follows from equation (5), using (6), (4) and (2) that

$$n_c(\mathbf{1},\mathbf{2}) = \omega(\mathbf{1})\,n(\mathbf{2}) + \omega(\mathbf{2})\,n(\mathbf{1}). \tag{7}$$

If we place point **1** in the X-channel and **2** in the Y-channel and integrate equation (7) over all sections of these channels which are *not* mutually shared, we find

$$n_c'(x,y) = n_s'(x)\,p'(y) + n_s'(y)\,p'(x), \tag{8}$$

where n_c' is the number of undesired pair coincidence counts per second, n_s' is n (see equation (1)) integrated over the unshared channel region, and p' is ω (see equation (2)) similarly integrated. The co-ordinate positions x and y are now the locations of the Y- and X-channels respectively, and thus also of the common region.

If $N_h(x,y)$ is the desired number of particle passages at the point (x,y) during an experiment of T sec duration, $N_c(x,y)$ the measured number of coincidences

in the experiment, $N_s(x)$ and $N_s(y)$ the corresponding total number of single passages through each channel, and $p(x)$ and $p(y)$ the corresponding presence numbers (occupation probabilities) of each channel, we have the following relations:

$$p(x) = p'(x) + T^{-1}\tau N_h(x,y), \tag{9}$$

$$N_s(x) = Tn_s'(x) + N_h(x,y), \tag{10}$$

$$N_c(x,y) = Tn_c'(x,y) + N_h(x,y) \tag{11}$$

(and corresponding equations for $p(y)$ and $N_s(y)$), from which, and equation (8), $N_h(x,y)$ can be found,

$$N_h(x,y) = \frac{N_c(x,y) - [N_s(x)\,p(y) + N_s(y)\,p(x)]}{1 - [p(x)+p(y)] - (\tau/T)\,[N_s(x)+N_s(y)-2N_h(x,y)]}. \tag{12}$$

In this equation $N_h(x,y)$ appears also in the last term of the denominator of (12), which is thus a quadratic equation for N_h. As the negative terms in the denominator are small compared with 1, N_h may be neglected, or replaced by N_c without serious error.

The value of τ to be used in (9) and (12) is essentially the value of τ at the point (x,y). As the mutually shared sensitive region is of finite dimensions, however, τ actually represents an average taken over this area.

The ratio τ/T is not measured directly. It depends on the thickness Δz of the sensitive volume, which however is independent of the concentration distribution and the position of the test cross-section along the z-axis. If we assume that the concentration near the input is constant and given by $C(x,y)_{z=0} = C_0$, we may write in zero approximation

$$p(x)_{z=0} = C_0 \Delta x \Delta z w_x, \quad N_s(x)_{z=0} = C_0 \Delta x \overline{V}(x) w_x T,$$

where w_x is the length of the channel and $\overline{V}(x)$ is the average velocity over the channel. We have therefore

$$\frac{\tau(x,y)}{T} = \frac{\Delta z}{TV(x,y)} = \left(\frac{p(x)}{N_s(x)}\right)_{z=0} \frac{\overline{V}(x)}{V(x,y)}, \tag{13}$$

and similarly

$$\frac{\tau(x,y)}{T} = \left(\frac{p(y)}{N_x(y)}\right)_{z=0} \frac{\overline{V}(y)}{V(x,y)}. \tag{14}$$

For our parabolic field of velocities we have

$$\frac{\overline{V}(x)}{V(x,y)} = \frac{2}{3}\frac{R^2-x^2}{R^2-(x^2+y^2)}, \quad \frac{\overline{V}(y)}{V(x,y)} = \frac{2}{3}\frac{R^2-y^2}{R^2-(x^2+y^2)}. \tag{15}$$

The expressions (13) and (14) with the help of (15) permit two independent determinations of the ratio τ/T in terms of magnitudes that our system is able to measure directly. As these calculations assume a constant particle distribution up to the wall of the tube it is preferable to make either x or y zero and to use either expression (13) or (14) respectively. This reduces the error due to finite particle dimension to the minimum.

We shall discuss in § 7 how allowance may be made for the fact that the signal duration $\tau(x,y)$ estimated as above may not correspond to the average τ needed in equation (12).

Let us note again that the denominator of expression (12) is but slightly sensitive to inaccuracies in the negative terms, which are always small with respect to 1. Much stronger is the influence of the experimental errors on the numerator in that formula, where in some instances the two terms

$$N_c \quad \text{and} \quad N_s(y)\,p(x)+N_s(x)\,p(y)$$

are almost equal and the difference is of the same order of magnitude as the errors. Although in principle the second term which depends on C^2 may be made very small by working at very low concentrations, the limitations of the apparatus make it undesirable to reduce the concentration by too much. The number of counts recorded in each passage would be low, requiring a high number of repetitions in order to increase the statistical data. The long time factor involved would make it difficult to assure constancy of conditions throughout all the measurements.

Bearing this in mind we have chosen concentrations as low as was practical for our experiments. We will discuss this point further in § 8.

The number of binary superpositions which occur within a single channel is of the same order as the number of pair coincidences between the two channels. The recorded number of 'singles' N_s is therefore smaller than the true number N_s^t of particles crossing the channel. A calculation on the same lines as that for n_c' thus gives the result

$$N_s^t(x) = N_s(x)/[1-p(x)]. \tag{16}$$

7. Effect of finite channel width in the derivation of concentration

In the majority of our experiments the width of the channels represent a sizable fraction of the tube diameter. On the other hand, the concentration gradients are in many instances very large, and localized in rather narrow intervals of the tube radius. A discussion will now be given of how the resolving power of our system was utilized to a fineness beyond the apparent coarseness of the scanning procedure.

Let us consider in the first place the effect of the finite dimensions Δx and Δy of the sensitive region in the case of a parabolic distribution of particle passages corresponding to a constant concentration C_0. The number of hits N_h will be proportional to the volume of suspension flowing through the area $\Delta x\,\Delta y$:

$$N_h = C_0 T \int_{x-\frac{1}{2}\Delta x}^{x+\frac{1}{2}\Delta x} \int_{y-\frac{1}{2}\Delta y}^{y+\frac{1}{2}\Delta y} V(x,y)\,dx\,dy.$$

Taking
$$V(x,y) = 2V_m[1-(x^2+y^2)/R^2],$$

we obtain
$$N_h = C_0 T[V(x,y) - V_m\{(\Delta x)^2+(\Delta y)^2\}/6R^2]\,\Delta x\,\Delta y.$$

The distribution deduced on the basis of N_h continues therefore to be parabolic and differs from the velocity distribution only by a constant correction. For instance, if $\Delta x = \Delta y = 2$ mm and $R = 5{\cdot}6$ mm, the resulting scanning error is 2 % of the counts at the centre of the tube. This is a systematic difference but its magnitude is negligible and in practice we have always neglected it.

In the case of a non-homogeneous distribution of the concentration, the blurring effect is much more serious, and a suitable computing method is necessary in order to go back from the counts (corrected according to formula (12)) to the local true concentration.

Let us restrict our analysis to the scanning of a diameter of the cross-section along the x-axis. If the distribution has radial symmetry, the gradient is directed along the x-axis, and we may neglect the variations in the transverse direction. Let us call

$$f(x) = C(x, 0)\, V(x, 0)\, T$$

the density of hits per unit area per experiment corresponding to the abscissa x. Note that $n = f/T$ (equation (1)). The number of hits corresponding to the area $\Delta x \Delta y$ around the point $(x, 0)$ will be

$$N_h(x) = \Delta y \int_{x-\frac{1}{2}\Delta x}^{x+\frac{1}{2}\Delta x} f(x)\, dx. \tag{17}$$

Displacing the position of the centre of the diaphragm from x to $x+\epsilon$, where $\epsilon \ll \Delta x$, the number of hits will change by the amount

$$N_h(x+\epsilon) - N_h(x) = \Delta y \epsilon [f(x+\tfrac{1}{2}\epsilon+\tfrac{1}{2}\Delta x) - f(x+\tfrac{1}{2}\epsilon-\tfrac{1}{2}\Delta x)].$$

From this we may deduce the recursion formulae:

$$f(x) = f(x-\Delta x) + \{N_h(x+\tfrac{1}{2}\epsilon-\tfrac{1}{2}\Delta x) - N_h(x-\tfrac{1}{2}\epsilon-\tfrac{1}{2}\Delta x)\}/\Delta y \epsilon, \tag{18}$$

$$f(x) = f(x+\Delta x) - \{N_h(x+\tfrac{1}{2}\epsilon+\tfrac{1}{2}\Delta x) - N_h(x-\tfrac{1}{2}\epsilon+\tfrac{1}{2}\Delta x)\}/\Delta y \epsilon. \tag{19}$$

From either of these formulae we can construct, step by step, the function $f(x)$ starting respectively from the periphery of the tube, where $f(x) = 0$, or from the centre, where N_h practically always has a very flat extremum. This implies that $f(x)$ also is practically constant for x close to zero and we may write

$$f(x) = N_h(x)/\Delta x \Delta y \quad \text{as} \quad x \to 0.$$

This analysis presupposes the knowledge of the parameters Δx and Δy. In fact, they were in general deduced from the experimental curves by a method of trial and error. One superimposes the distributions that result independently from (18) and (19) and changes the parameters Δx and Δy until as good a fit as possible is obtained.

Some simplifications of the problem are possible. For example, Δx and Δy may be treated as identical, which is permissible if the two discrimination levels have been carefully matched. In some special cases, moreover, the determination of Δx is particularly simple: (*a*) when the distribution is strictly parabolic; in this case the knowledge of the bulk concentration C_0 and the number of hits at the centre of the tube allows us to write

$$(\Delta x)^2 = N_h(0, 0)/2C_0 V_m T;$$

(*b*) when the concentration distribution is sharp; in this case the plot of N_h will show two very steep portions, whose distance apart on the x-axis is just the value of Δx in which we are interested (figures 9 and 11).

A final adjustment or check involves a back calculation of the N_h-curve from the f-distribution obtained and comparison of it with the data. Similarly, f may be integrated over the cross-section and the integral compared with the known throughput of particles.

We recall the problem already mentioned concerning the value of τ/T to be introduced in formula (12). As was pointed out the value of this parameter at (x, y) may differ from the average value in the region $\Delta x \Delta y$, which is required in equation (12). To estimate this we employ a first rough evaluation of the distribution $f(x)$ and calculate as the value to be used

$$\langle \tau/T \rangle = \sum_{\Delta x} f(x')\, \tau/T \Big/ \sum_{\Delta x} f(x') \quad (x' = x, x \pm \epsilon, x \pm 2\epsilon, \ldots),$$

where the summation extends over the range Δx around x.

In view of the fact that there is central symmetry about the tube axis at all cross-sections (a fact which we have verified, see next section) we are interested in f as a function of the radial position r only, where $r = (x^2+y^2)^{\frac{1}{2}}$. Our results therefore will be reported in terms of r. Note, moreover, that

$$f(r) = T\, V(r)\, C(r).$$

In order to derive $C(r)$ we must divide f by TV where, as already mentioned,

$$V = 2V_m[1-(r/R)^2]$$

and $TV_m = 670$ cm is a constant of the apparatus.

8. Controls and discussion of typical results

(*a*) *Symmetry about the axis and reproducibility*

In a preliminary survey of the performance of the apparatus the symmetry of the distribution around the axis of flow has been checked by scanning along the two perpendicular diameters $x = 0$ and $y = 0$ and at intermediate positions where neither x nor y were zero. These controls showed that the proper positioning of the stirrers was important and great care was always exercised to avoid errors due to this. In subsequent measurements the scanning was confined to both positive and negative values of x along the diameter $y = 0$.

We also tested the effect of variations of the shape of the conical section leading from the supply container to the flow tube. The results were found to be unaffected by a widely differing choice of angle for the entrance cone.

A typical series of measurements is shown in table 1. Every 'experiment' is composed of ten successive measurements of N_c while the N_s values are determined once for channel X and once for channel Y, that is five times each. We indicate by a number preceded by the letter S a series of such experiments, performed as just mentioned, and covering all positions along a diameter for a certain set of flow conditions, choice of l and discrimination level, i.e. Δx. In the table we give only the averages with their standard errors. The only inconsistency between the results of positive and negative x values appears around about $x = 2{\cdot}5$ mm. Here, however, we are in a region of very steep variation of counts, which more than

double in a displacement of the scanning position by half a millimetre. Slight misplacements of the diaphragm can thus lead to appreciable differences between results.

Downward flow: distance from tube mouth $l = 120$ cm, flow time $T = 10$ sec, particle diameter $2a = 1{\cdot}21$ mm, concentration $C_0 = 2$ cm^{-3}, fluid viscosity = 340 cP, $\Delta x = 1{\cdot}9$ mm.

Experiment no.	r	$N_{sr}(0)$	$N_{sx}(r)$	$N_c(0, r)$
842	0	235 ± 5	236 ± 5	$24{\cdot}4 \pm 1{\cdot}3$
865	0	225 ± 6	236 ± 6	$27{\cdot}5 \pm 2{\cdot}0$
841	$-0{\cdot}5$	247 ± 5	246 ± 10	$27{\cdot}4 \pm 1{\cdot}0$
864	$+0{\cdot}5$	238 ± 3	246 ± 13	$27{\cdot}0 \pm 1{\cdot}9$
828	$-1{\cdot}0$	251 ± 3	244 ± 6	$31{\cdot}1 \pm 1{\cdot}9$
840	$-1{\cdot}0$	246 ± 3	251 ± 8	$25{\cdot}2 \pm 1{\cdot}7$
863	$+1{\cdot}0$	240 ± 11	256 ± 7	$30{\cdot}1 \pm 2{\cdot}5$
837	$-1{\cdot}5$	246 ± 11	258 ± 8	$27{\cdot}9 \pm 1{\cdot}9$
862	$+1{\cdot}5$	242 ± 5	257 ± 7	$33{\cdot}1 \pm 1{\cdot}7$
836	$-2{\cdot}0$	$238 \pm 4{\cdot}5$	295 ± 6	$41{\cdot}6 \pm 1{\cdot}6$
861	$+2{\cdot}0$	249 ± 6	292 ± 4	$37{\cdot}6 \pm 1{\cdot}6$
835	$-2{\cdot}25$	240 ± 9	327 ± 9	$45{\cdot}6 \pm 1{\cdot}9$
860	$+2{\cdot}25$	$240 \pm 7{\cdot}5$	309 ± 8	$43{\cdot}3 \pm 2{\cdot}0$
833	$-2{\cdot}5$	252 ± 8	365 ± 8	$103{\cdot}1 \pm 1{\cdot}0$
859	$+2{\cdot}5$	243 ± 12	348 ± 8	$74{\cdot}4 \pm 3{\cdot}2$
866	$+2{\cdot}5$	$244 \pm 4{\cdot}5$	$327 \pm 3{\cdot}5$	$60{\cdot}0 \pm 2{\cdot}4$
832	$-2{\cdot}75$	$235 \pm 4{\cdot}5$	342 ± 7	$87{\cdot}0 \pm 2{\cdot}9$
834	$-2{\cdot}75$	253 ± 9	379 ± 9	$131{\cdot}0 \pm 3{\cdot}8$
858	$+2{\cdot}75$	$223 \pm 9{\cdot}5$	$360 \pm 5{\cdot}5$	$107{\cdot}0 \pm 3{\cdot}7$
867	$+2{\cdot}75$	223 ± 5	361 ± 4	$103{\cdot}9 \pm 3{\cdot}3$
831	$-3{\cdot}0$	260 ± 5	$379 \pm 7{\cdot}5$	$129{\cdot}1 \pm 2{\cdot}3$
857	$+3{\cdot}0$	237 ± 9	$343 \pm 13{\cdot}5$	$119{\cdot}6 \pm 4{\cdot}3$
830	$-3{\cdot}25$	243 ± 4	346 ± 9	$130{\cdot}2 \pm 3{\cdot}7$
856	$+3{\cdot}25$	266 ± 3	322 ± 10	$127{\cdot}7 \pm 4{\cdot}1$
829	$-3{\cdot}5$	$255 \pm 7{\cdot}5$	293 ± 9	$124{\cdot}7 \pm 3{\cdot}7$
855	$+3{\cdot}5$	239 ± 8	281 ± 6	$114{\cdot}7 \pm 4{\cdot}3$
843	$-3{\cdot}75$	248 ± 6	238 ± 5	$111{\cdot}7 \pm 2{\cdot}2$
854	$+3{\cdot}75$	$234 \pm 4{\cdot}5$	$250 \pm 10{\cdot}5$	$105{\cdot}8 \pm 3{\cdot}9$
844	$-4{\cdot}0$	237 ± 6	$205 \pm 14{\cdot}5$	$105{\cdot}6 \pm 3{\cdot}7$
853	$+4{\cdot}0$	231 ± 4	190 ± 5	$100{\cdot}3 \pm 8{\cdot}1$
845	$-4{\cdot}25$	241 ± 9	134 ± 4	$93{\cdot}6 \pm 2{\cdot}8$
852	$+4{\cdot}25$	240 ± 9	129 ± 5	$82{\cdot}4 \pm 4{\cdot}7$
846	$-4{\cdot}5$	265 ± 10	$43{\cdot}3 \pm 7$	$41{\cdot}7 \pm 3{\cdot}8$
851	$+4{\cdot}5$	236 ± 8	$61{\cdot}0 \pm 3$	$55{\cdot}4 \pm 2{\cdot}0$
847	$-4{\cdot}75$	—	0	0
850	$+4{\cdot}75$	—	0	0
848	$-5{\cdot}0$	—	0	0
849	$+5{\cdot}0$	—	0	0

TABLE 1. Experimental data for series S. 14.

Systematic misplacements of the diaphragm zero position have also been observed. In figure 8, for example, two full series of experiments are shown performed under identical conditions but some weeks apart in time during which

the apparatus was disassembled and the suspension replaced. The first series are represented by points + and − depending on whether the scanning position was to the right or left of the tube centre and the second series by points ⊕ and ⊖ similarly defined. All points can be brought to almost perfect superposition by systematic shifts of the zero $+\frac{1}{8}$ mm for the first series and $-\frac{1}{8}$ mm for the second.

We may conservatively assume that the error on the abscissa is never larger than 0·25 mm in single experiments and 0·2 mm on the average. As for the errors on the ordinate, excluding the regions of steep variations, we see that they are of the order of ± 4 % for the average N_c values, while the dispersion of the points around these averages is of the order of ± 6 %. The results for N_s are of course much better.

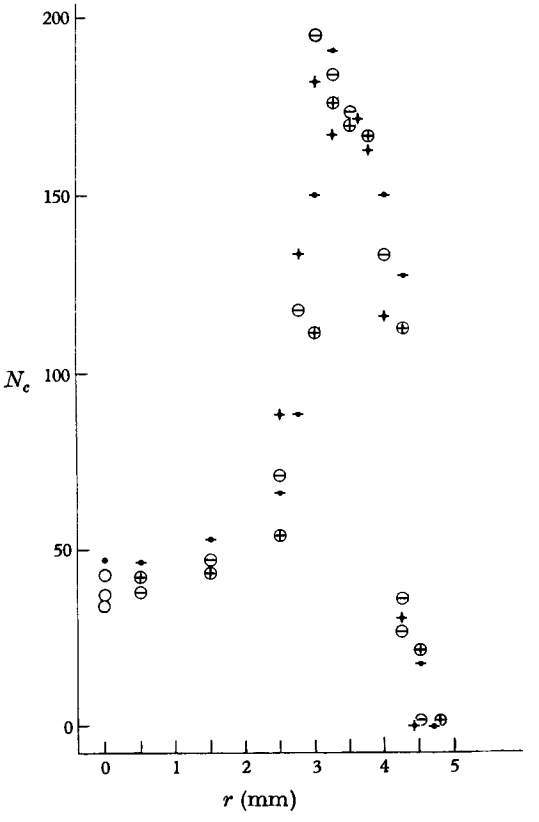

FIGURE 8. Uncorrected coincidence counts N_c for series S. 18A and S. 18B; dependence on radial position r. Concentration $C_0 = 4$ cm^{-3}; $\Delta x = 1{\cdot}5$ mm; other variables as for S. 14, see table 1. −, S. 18A left of tube centre; +, S. 18A right of tube centre; ⊖, S. 18B left of tube centre; ⊕, S. 18B right of tube centre; •, S. 18A centre; ○, S. 18B centre. N_c is the number of counts during the passage of the total test volume.

The reproducibility of the presence numbers p has also been checked by repeating the same series of measurements at different times: in general the reproducibility was worse than that for N_s and N_c, in the sense that, upon repeating a series, the resulting distributions, while always very similar in shape, nevertheless have shown relative deviations by as much as 15 %. Taking into

consideration that the presence numbers depend also on Δz, which is rather sensitive to the optical and electronic conditions, the appearance of systematic discrepancies is understandable. The probable error in p was thus set at $\pm 10\,\%$ in all cases.

An uncertainty of the same order is present also in the value of τ, but this matters very little. The total error resulting in the calculation of N_h from the denominator in formula (12) is never larger than 2 %. The total errors in N_h are typified by the ranges shown in figures 9 and 11.

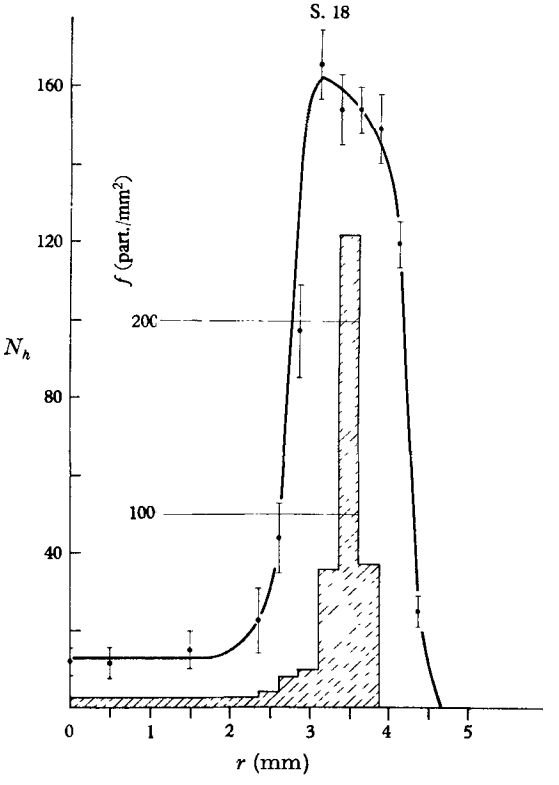

FIGURE 9

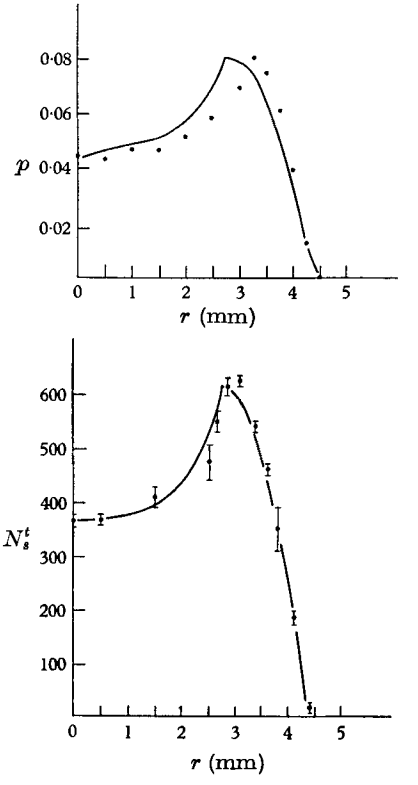

FIGURE 10

FIGURE 9. Derived hit coincidence counts N_h and hit density f for series S. 18; dependence on radial position r. The lines indicate the standard error in N_h. Full line: reconstructed curve of N_h using the f-histogram shown. N_h and f refer to the passage of the total test volume.

FIGURE 10. Presence number p and total number of single passages N_s^t as a function of radial position r for series S. 18. Points are the experimental results; lines are the reconstructed curves using the f-histogram of figure 9. N_s^t refers to the passage of the total test volume.

Figure 9 shows the relation between the N_h values (points) and the function f, computed from the data as explained in § 7 and represented by the hatched histogram. The full curve in the figure is obtained by integration of the histogram according to equation (17) and checks very well with the experimental points.

A further important check is made by reconstructing, by numerical integration,

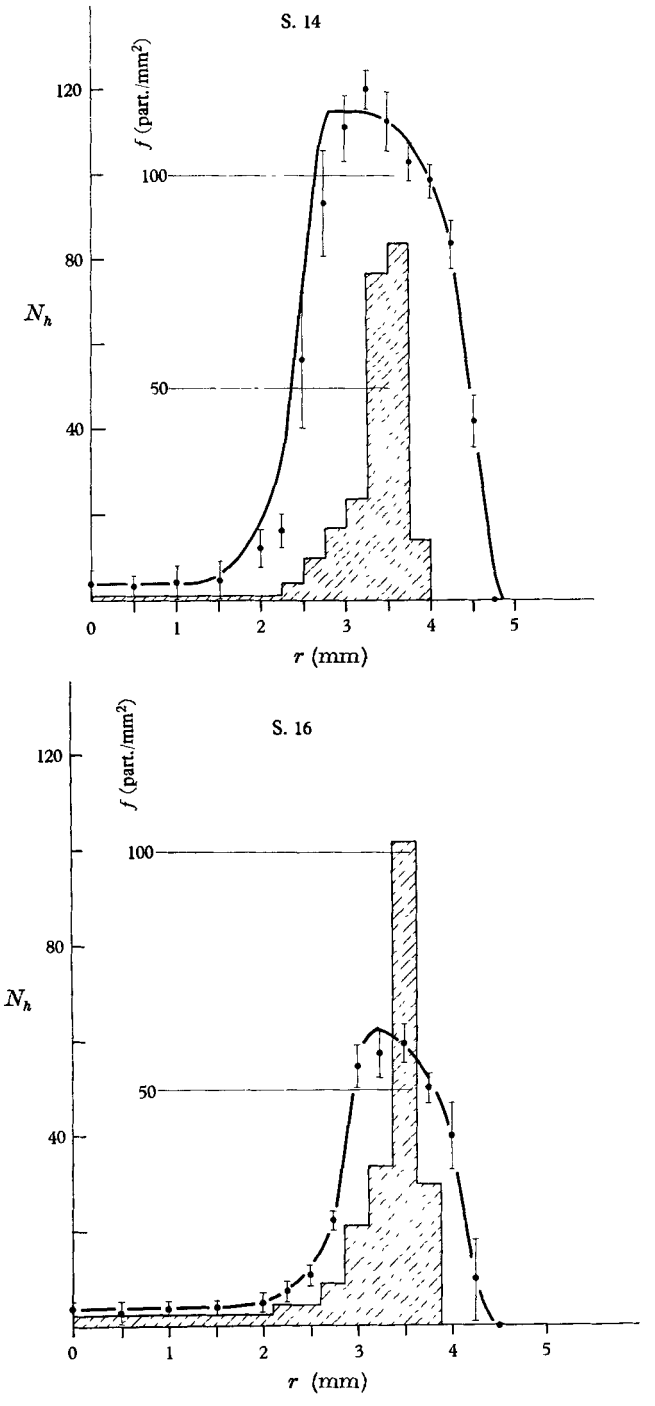

FIGURE 11. Derived hit coincidence count N_h and hit density f for series S. 14 and S. 16; dependence on radial position r. (For data in case S. 14 see table 1; S. 16 has been performed under the same conditions but with smaller Δx.) Standard errors in N_h are indicated. Full lines reconstructed from f. Note that the two f-histograms match since f is independent of discrimination level. As the flow condition in series S. 18, figure 9, were similar, the histograms in figure 9 can also be compared with the above. Note however that series S. 18 was done at double the concentration of series S. 14 and S. 16.

the curves of the singles N_s^l and of the presence numbers p from the f distribution obtained (figure 10).

(*b*) *Effect of the channel width* Δx

Some series of measurements have been repeated with two different discrimination levels, resulting in different channel widths Δx. The reduction in the area of the sensitive region reduces the total count, and in the same proportion reduces

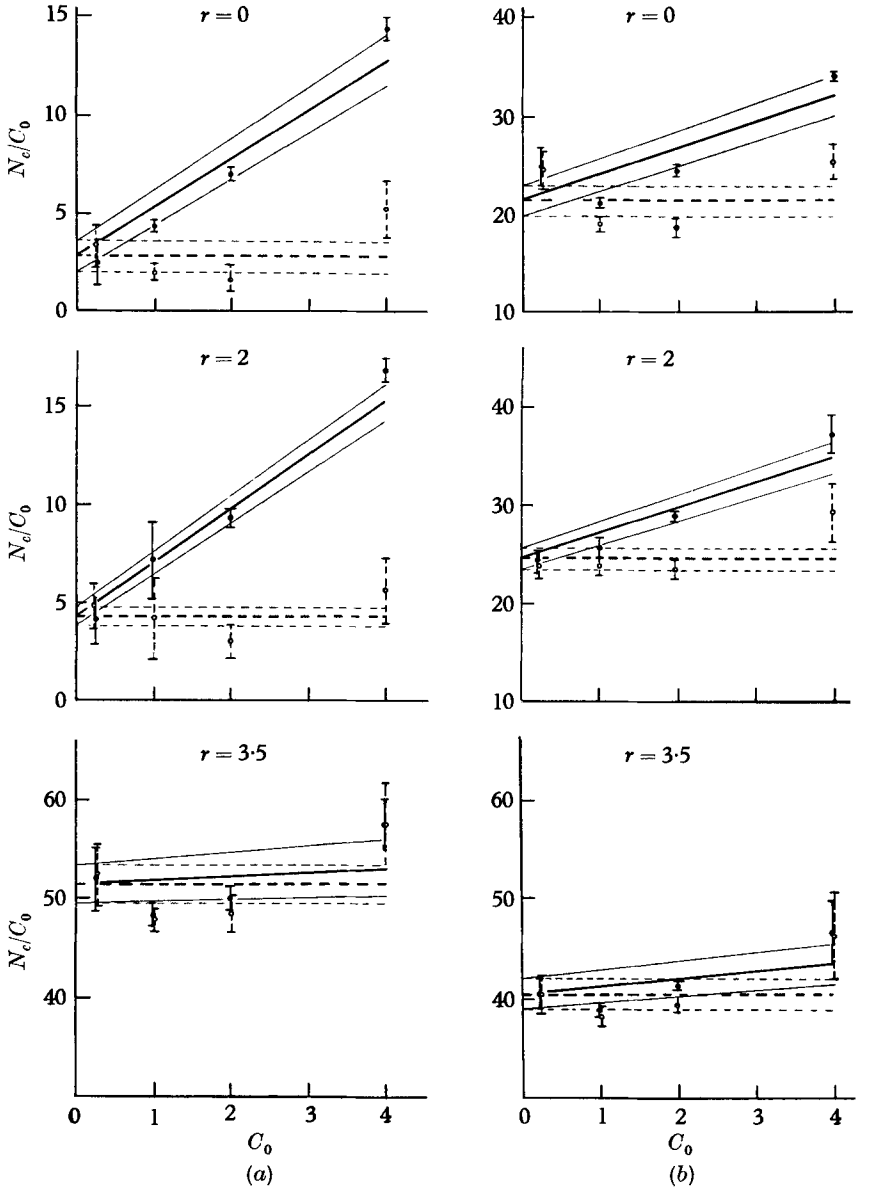

FIGURE 12. Concentration dependence of reduced total and hit coincidence counts for two L_3-values (see Part 2). (*a*) $L_3 = 8{\cdot}6$ downwards; (*b*) $L_3 = 2{\cdot}2$ upwards. ●, N_c/C_0; ○, N_h/C_0. Full heavy line, derived from equation (20). Intercept level shown by heavy dotted line gives N_h/C_0-value expected. Thin lines are confidence limits.

the number of pair coincidences. The f-distribution, however, which depends only on the flow variables, should be the same in both cases. The results of two such series of measurements are shown in figure 11. Such differences as occur in the f-distribution near its maximum fall within the precision that we may expect in the determination of r. The relatively large difference in the region of small r values is probably due to the large error associated with the numerator of equation (12).

The total area bounded by the f-distribution and the r-axis should be nearly equal to the number n of particles entering the tube during an experiment. In the case of figure 11, $n = 1320$, as the flow volume is 660 cm^3 and the concentration C_0 is 2 part./cm^3.

The values obtained by integration are $n = 1240$ for S. 14, and $n = 1120$ for S. 16. The agreement may be regarded as rather satisfactory.

(c) *Concentration dependence*

A change in the bulk concentration C_0 may affect the number of counts both due to particle interaction and for statistical reasons. In order to separate these two questions, we will first assume that no interaction between the particles occurs, so that the concentration at any point in the flow tube is due to a linear superposition of independent particle trajectories. This is justified at the low concentration at which we are working, as we will prove more precisely later.

In this case N_h, N_s' and in first approximation also p and N_s are proportional to C_0. We have thus $N_h = N_h^0 C_0$, $p = p^0 C_0$, $N_s = N_s^0 C_0$, where N_h^0, p^0 and N_s^0 are the values corresponding to $C_0 = 1$.

We now want to check the statistical analysis of § 6. From equation (12) we have upon rearranging

$$N_c = N_h^0 C_0 + [N_{sy}^0 p_x^0 + N_{sx}^0 p_y^0 - N_h^0 (p_x^0 + p_y^0) - (\tau/T)\, N_h^0 (N_{sx}^0 + N_{sy}^0)]\, C_0^2 \qquad (20)$$

and the plot of N_c/C_0 *vs* C_0 should be a straight line.

This has been checked using four different concentrations from $C_0 = 0{\cdot}25$ to $C_0 = 4$ part./cm^3, at three distances from the axis and two flow conditions. In figure 12 are shown, plotted against concentration C_0, the results for N_c/C_0 and for N_h/C_0, where N_h was calculated from (12). The heavy full lines are the representations of equation (20), using for slope and intercept the average values for the four concentrations. The confidence limits indicated by the thin lines are derived from the standard errors of the different measurements. The horizontal dotted lines give the expected level for N_h/C_0. The agreement between the lines and the experimental points is only approximate and there are indications that the highest concentration used may be on the border of what is permissible.

In order to demonstrate that the particle distributions are concentration-independent (within the range in which we are working) we have repeated the complete scanning for some hydrodynamic situations at two different concentrations, and the corresponding concentration distributions always agree very well.

Figures 11 and 9, which show one of these checks, correspond respectively to $C_0 = 2$ and $C_0 = 4$ part./cm^3. No significant difference seems to be present in the histograms representing the f-distribution. Other comparisons have been made

at lower concentrations and under different flow conditions. The comparison of the N_h values for two series S. 7 and S. 9, corresponding to particles of smaller radius and at concentrations $C_0 = 1$ and $C_0 = 2$ part./cm^3 respectively is illustrated in Part 2 (figure 4) of this paper. In these experiments no concentration gradients have yet developed, and the distributions are very nearly parabolic (note that N_h is plotted against r^2).

In connexion with parabolic distributions we should mention a relation which is satisfied between the counts of singles and of hit coincidences at the centre, independently of Δx:

$$[N_s^l(0)]^2/N_h(0,0) = (32/9)V_m T R^2 C_0 = 750 C_0.$$

This relation besides being a check on the counting performance may be considered also as a control upon the concentration actually present. For the two series just mentioned we obtain

$$[N_s^l(0)]^2/N_h(0,0) = 615 \quad \text{and} \quad [N_s^l(0)]^2/N_h(0,0) = 1335,$$

i.e. $C_0 = 0{\cdot}82$ and $1{\cdot}78$ respectively. The fact that C_0 as measured here is somewhat smaller than the nominal concentration may be due to some of the particles not being sufficiently opaque to be recorded.

9. Conclusion

It has been shown that the apparatus described is capable of delivering significant data for the number of particle passages per unit time at any level in the tube and at any point of the cross-section. We have examined the limits of reliability which, though they vary somewhat with conditions, are at all times such that the 'tubular pinch' effect described in Part 2 can be regarded as established in the cases which we have considered.

While this technique cannot resolve the product of 'particle concentration' times 'local flow velocity' it is reasonable to assume that the flow pattern remains parabolic in all cases here considered. Direct evidence for this may be seen in the parabolic distribution measured near the tube mouth and from certain other experiments where particle velocity and position have been measured directly.

In this sense therefore the method allows one to calculate particle concentration everywhere in the tube and from it, as will be shown in Part 2 (Segré & Silberberg 1962), conclusions may be drawn about the particle trajectory.

Acknowledgements are due to Mr M. Nutman of the Weizmann Institute who made the difficult glass parts of the apparatus.

REFERENCES

SEGRÉ, G. & SILBERBERG, A. 1961 *Nature, Lond.*, **189**, 209.
SEGRÉ, G. & SILBERBERG, A. 1962 *J. Fluid Mech.* **14**, 136.